Politecnico di Torino

Porto Institutional Repository

[Proceeding] CFD MODELING OF SOLAR COLLECTOR WITH NANO-FLUID DIRECT ABSORPTION FOR CIVIL APPLICATION

(Article begins on next page)
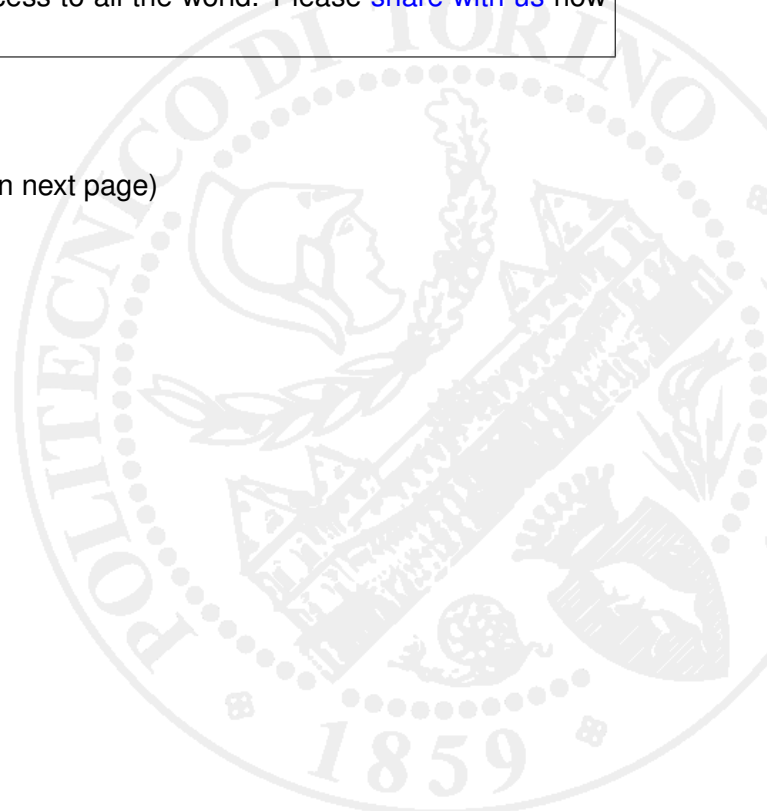
CFD MODELING OF SOLAR COLLECTOR WITH
NANO-FLUID DIRECT ABSORPTION FOR CIVIL APPLICATION

A. Moradi[a], E. Sani[b], M. Simonetti[a]*, F. Francini[b], E. Chiavazzo[a], P. Asinari[a]

[a] Energy Department, Politecnico di Torino, corso Duca degli Abruzzi 24 10129, Torino, Italy,

[b]National Institute of Optics, National Research Council (CNR-INO), largo E. Fermi 6 50125, Firenze, Italy

*corresponding author: marco.simonetti@polito.it

ABSTRACT

Direct solar absorption has been considered often in the past as a possible configuration of solar thermal collectors for residential and small commercial applications. Of course, a direct absorption could improve the performance of solar collectors by skipping one step of the heat transfer mechanism of standard devices and by modifying the temperature distribution inside the collector. In fact, classical solar thermal collectors have a metal sheet as absorber, designed such that water has the minimum temperature in each transversal section, in order to collect as much as possible the solar thermal energy. On the other hand, in a direct configuration, the hottest part of the system is the operating fluid and this allows to have a more efficient conversion. Nanofluids, i.e. fluids with a suspension of nano-particles, as carbon nano-horns, could be a good and innovative family of absorbing fluids, for their higher absorption coefficient with respect to the base fluid and stability under moderate temperature gradients. Moreover, carbon nanohorns offer the significant advantage to be non-toxic unlike other carbon nanoparticles (e.g. carbon nanotubes). In this work, an original 3D model of the absorption phenomena in nano-fluids flowing in a cylindrical tube is coupled with a CFD analysis of the flow and temperature field. Recent measurements of the optical properties of nano-fluids with different concentrations have been used for the radiation heat transfer modeling and included in the fluid dynamic modeling as well. Heat losses due to conduction, convection and radiation at the boundaries are included in the model. The results are compared with the typical performance of flat solar collectors present on the market.

Keywords: nanofluids, solar direct absorption, CFD, evacuated tube solar collector

INTRODUCTION

The "20-20-20" EU's strategy [1] fixed a target of 20% share of renewable energy on the year 2020's horizon for Europe. In 2009 renewable energy share (all renewable technology, both electrical and thermal) for environmental heating and cooling was 13.4% for EU-27 (8.2% for Italy) (Eurostat 2012). The heating and cooling demand are solved with different shares of electricity and thermal sources among EU countries, nonetheless distributed thermal renewable energy tecnologies play an important role in the general strategy of reducing environmental footprint.

A better exploitation of solar thermal technology is considered in the actual European energy target for 2020. National Renewable Energy Action Plans point to a share of 6% of the EU-27 heating and cooling demand matched by solar thermal technology [2].

The UK Government definition of Microgeneration [3] applies to heat and power generating technologies with a thermal output below $45kW_t$ or an electrical output of $50kW_e$. It covers electrical generation from wind, solar photovoltaics (PV) and hydro, and heat generation from biomass, solar thermal and heat pumps as well as micro combined heat and power (CHP), which produce heat and power from renewable or fossil fuels, expecially considering low carbon technologies.

Other countries, such as Italy [4], have more restrictive legal definition, considering only electrical energy production and cogenerative plants, again of low power.

In the near past, some interesting investigations, among which those in Ref. [5], reported that renewable energy adoption is significantly valued by households, but this value is not sufficiently large to cover the higher capital costs of micro-generation energy technologies (at least, for the vast majority of households).

Hence new solutions should be explored, in order to improve the diffusion of solar thermal microgeneration systems. In this paper, we

focus on new materials for solar thermal collectors, mainly aiming to become low-cost industrialized products in the near future. We focused on microgeneration in civil low temperature applications, such as domestic hot water production and indoor environmental heating.

A basic idea may be to save production costs by introducing plastic materials. This could be a plus also from a point of view of embodied energy and LCA, for example presented in Ref. [6], but this point is still under investigation. Low temperature direct absorption may be promising for the application of plastic (transparent) materials, because it avoids the problems due to low thermal conductivity and conversely the latter property may actually promote thermal insulation.

The use of novel dark fluids for direct absorption has been recently considered. Nanofluids, i.e. fluids with a suspension of nano-particles, as carbon nano-horns, could be a good and innovative family of absorbing fluids, for their higher absorption coefficient with respect to the base fluid and stability under moderate temperature gradients. Their possible uses in solar thermal system have been recently reviewed in Ref. [7].

In this paper we present a 3-D model to study the application of single-wall carbon nanohorn-based nanofluid in a cylindrical tube collector.

The anisotropic nature of cylindrical tube collectors yields angularly dependent optical efficiencies [8]. Hence, in cylindrical configuration, the choice of transparent materials to construct tube strongly depends on the optical properties of the material. Moreover, choosing transparent materials depends on thermal, physical and mechanical properties of the materials and also requires economical considerations. Plastic materials are cheaper than glass, so they may decrease the cost of production. They also have lower thermal conductivity, which increases thermal resistance and lowers heat loss. Furthermore, they are not broken by hail or stones, and, in the form of thin films, they are completely flexible and have low mass. However, they are generally limited in the temperatures they can sustain without deteriorating or undergoing dimensional changes and many of them cannot withstand the sun ultraviolet radiation for long periods [9].

In this study three different materials are considered and compared each other: PMMA, as an example of plastic materials, fused silica and borosilicate glass. The paper is organized as follows: firstly, numerical investigations are presented, describing modeling assumptions and boundary conditions; then experimental measurements of optical properties are introduced, followed by a *Results and discussion* paragraph. *Comments* are reported in a dedicated paragraph. Finally, the work is summarized in the *Conclusions* section.

NUMERICAL INVESTIGATIONS

Modelling methods and configurations

A three-dimensional numerical simulation of the nanofluid-based solar receiver is performed by using commercial CFD software FLUENT™ and a user defined function (UDF) has been developed in order to include radiation absorption and transmittance of the glass in the modelling.

Numerical modelling is performed for single tube receiver without insulation, in the presence of natural convection and forced convection.

Governing Equations

Since the Reynolds number for the considered maximum inlet velocity is still in laminar flow regime, the laminar flow model is used. So, the governing equations for modelling the internal flow of nanofluid and the temperature distribution are as follows:

Continuity equation:

$$\nabla \cdot (\rho \vec{v}) = 0$$
(1)

Momentum equation:

$$\nabla \cdot (\rho \vec{v} \vec{v}) = \nabla \rho + \nabla \cdot (\bar{\tau}) + \rho \vec{g}$$
(2)

Energy equation:

$$\nabla \cdot (\rho \vec{v} h) = \nabla \cdot k(\nabla T) + q_h$$
(3)

$\bar{\tau}$ Is the stress tensor and is given by:

$$\bar{\tau} = \mu \left[(\nabla \vec{v} + \nabla \vec{v}^T) - \frac{2}{3} \nabla \cdot \vec{v} I \right] \qquad (4)$$

In order to compute the energy source in the energy equation, the Radiative Transport Equation (RTE) for the total radiation intensity (integrated over wavelengths) has been solved.

$$dI = I \cdot \propto_m \cdot dr \qquad (5)$$

$\propto_m$ is the mean absorption coefficient and is obtained by the average of the spectral absorption coefficient weighted by the spectral solar irradiance:

$$\alpha_m = \frac{\int_0^\infty I_\lambda . \alpha_\lambda . d\lambda}{\int_0^\infty I_\lambda . d\lambda} \tag{6}$$

I_λ is the spectral intensity of the radiation entering fluid and is obtained by:

$$I_\lambda = I_{sun,\lambda} . \tau_\lambda \tag{7}$$

Where τ_λ is the spectral transmittance of the tube's wall. RTE equation shows the attenuation in the radiation intensity as it passes through the fluid so it is equal to the intensity absorbed by the fluid. Then, energy absorbed by the cell volume is obtained by:

$$d\emptyset = I . \alpha_m . dr . dA = I . \alpha_m . dV \tag{8}$$

So the volumetric energy source is obtained by the following experession:

$$q_h = \frac{d\emptyset}{dv} = I . \alpha_m \tag{9}$$

Local radiation intensity can be obtained using Lambert's law, which is a solution to RTE equation (eq.5):

$$I = I_{sun} . \tau_x . \exp(-\alpha . r) \tag{10}$$

where I_{sun} is the sun's irradiance which Is considered to be equal to 1000 W/m^2 and I is the total radiation intensity passed through the glass.

$$I_{sun} = \int_0^\infty I_{sun\_\lambda} . d\lambda \tag{11}$$
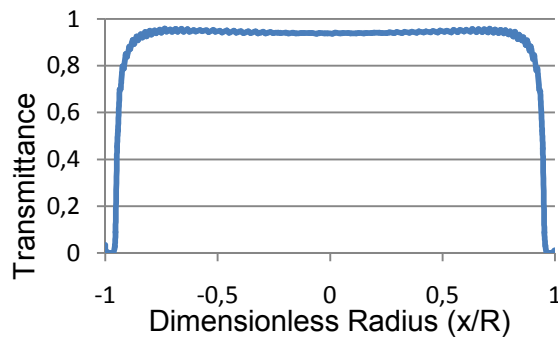

Figure 1: the transmittance as a function of dimensionless radius, τ_x

Figure 1 shows the τ_x the transmittance of the glass as a function of x coordinate. Using the data obtained for the transmittance of the 3 tube materials, for each of them, the data is divided into 3 regions for higher accuracy and then τ_x function is approximated by a 6th order polynomial using least square method. The overall value of the transmittance is different

less than 1% for the three materials we used: PMMA, fused silica and borosilicate glass.

$$\tau_x = P_7 + P_6 x^6 + P_5 x^5 + P_4 x^4 + P_3 x^3 + P_2 x^2 + P_1 x^1 \tag{12}$$

Heat loss analysis

Let us consider the non-symmetric setup in order to compute the overall heat loss coefficient. First of all, the external radiation temperature for upper and lower halves of the collector are different. Secondly, in the case of natural convection, heat transfer coefficient depends on surface temperature and this coefficient would be different for the upper and lower half of the collector, due to a considerable difference in the their temperatures. Therefore, the collector is divided into upper and lower half and heat loss coefficient for each half is calculated separately.

The tube containing the nanofluid is in direct contact with the ambient. The heat loss occurs by convection to the ambient and radiative loss from the upper half to the sky and from the lower half to the roof.

Convective loss to the ambient is considered under two circumstances. Firstly, in the presence of wind with speed equal to 5 m/s [10]. In this case, convective heat loss coefficient is constant and is not dependent on the surface temperature. Secondly, when natural convection is dominant, the heat loss coefficient is temperature dependent and is calculated by empirical relation for horizontal cylinders [11].

$$h_a = \frac{k_a . D_o}{Nu} \tag{13}$$

$$Nu = \left\{ 0.6 + \frac{0.387 \times (Ra)^{1/6}}{\left[1 + (\frac{0.559}{Pr})^{9/16} \right]^{8/27}} \right\} \tag{14}$$

Here, D_o is the outer diameter of tube, Nu is the nusselt number, Pr is the prantdl number, k_a is the thermal conductivity of the air and Ra is the Rayleigh number. All of these values are evaluated at the mean temperature of the outer surface and the ambient temperature.

Radiation loss is divided into two parts:

- From the lower half of the cylinder which exchange the heat with roof in thermal equilibrium with the ambient (T_{roof} =288.15 K)
- From the upper half of the roof which exchanges heat with the sky

A simple correlation could be used to estimate the apparent sky-temperature [12].

$$T_{sky} = 0.0552 T_a^{1.5} \qquad (15)$$

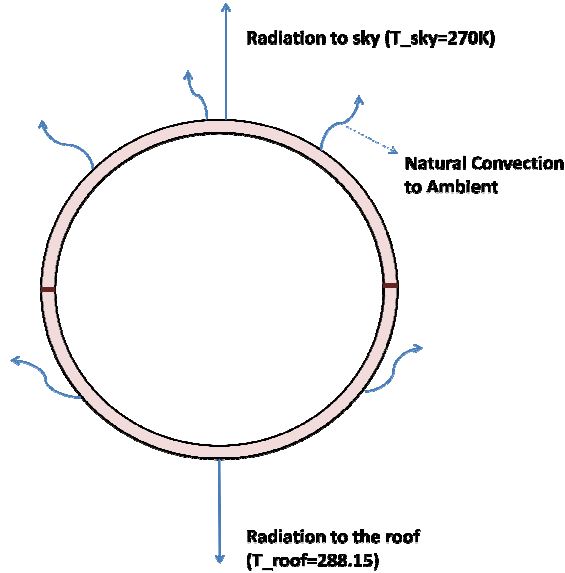Figure 2 schematically shows heat loss from the single tube solar collector to the ambient.

Figure 2: Radiative and convective heat loss from single tube solar collector to the ambient

Irradiation UDF

In order to find the value of local volumetric energy source in eq. (3), a User Defined Function (UDF) is developed and incorporated into FLUENT™. This UDF uses the position of cell center to find volumetric source intensity. Intensity of local volumetric energy source is determined by:

- Radiation extinction according to the Lambert's law, which requires finding the length of the light path r in eq. (10), before hitting the cell. The length of the light path is obtained using the position of the volume cell center, as depicted in Figure 3.
- Change in transmittance τ_x , used in eq, (10), due to optical extinction of the tube, shown in figure 1. Position of the cell center on the x axis is used, then corresponding value of τ_x is taken from the τ_x function.
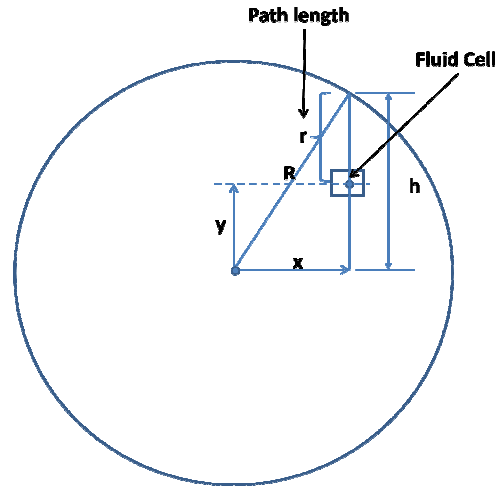

Figure 3: Geometrical construction for finding the length of the light path hitting the cell.

Geometry and Grid Generation

The geometry was chosen on the basis of a typical evacuated solar collector, with 1.8 m length and 0.0438 m inner diameter. Since Lambert's equation is a convex function, using the cell center position to find local value of radiation intensity underestimates the real value of the average intensity inside the cell. Hence, even though the fluid dynamics and heat transfer characteristics of the fluid can be simulated by a coarser mesh, a fine mesh is needed to find a more precise value for the energy source.

Hence a Matlab™ code is written to find the error introduced in the source term for different meshes for a path length of 2.5 centimeter. The results for 3 different meshes are compared in Figure 4. For the mesh with interval count equal to 50 the error is so close to zero.
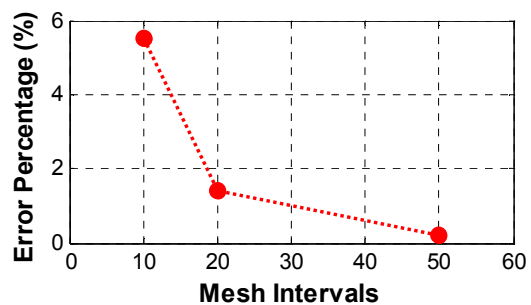

Figure 4: Error introduced by assumption of the cell center distance for different mesh sizes

Finally the proper mesh for the 3D geometry is validated by performing energy balance for the considered mesh.

EXPERIMENTAL STUDY AND SIMULATION OF OPTICAL PROPERTIES

Optical properties of nanofluids

Optical transmittance spectra at room temperature is measured using a double-beam UV–VIS spectrophotometer (PerkinElmer Lambda900). The nanofluid is hold in 10-mm path length quartz cuvettes.

Table 1: Samples under investigation. A-samples and G-samples refer to water-based or glycol-based suspensions, respectively

Label	SWCNH Concentration (g/L)
A3	0.004
A4	0.006
A5	0.010
A6	0.020
A7	0.050
G3	0.050

For a more meaningful characterization of nanofluids, the transmittance of the pure base fluids (water or ethylene glycol) is also measured as a reference. The acquired transmittance spectra are corrected for the reflectance term according to the formalism developed in Ref. [13]. The absorption coefficient is obtained from measurements keeping into account the light scattering albedo, as detailed in Ref [14].
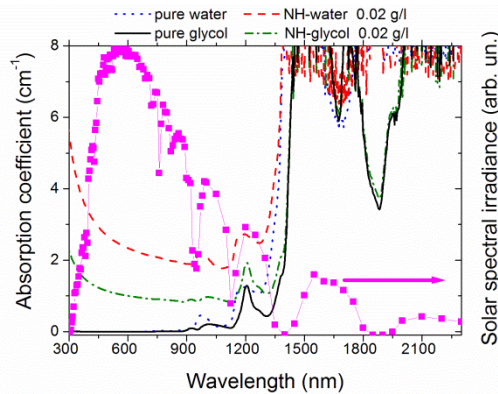

Figure 5: Spectral absorption coefficient of nanofluids and base fluids. The sunlight spectral irradiance for air mass 1.5 is superimposed to the spectra for reference.

Figure 5 shows a comparison of the spectral absorption coefficients of nanohorn suspensions in water and ethylene glycol. The spectral absorption coefficient of pure base fluids is also shown for reference. The sunlight spectrum with air mass 1.5 is also depicted in the figure, making immediately evident the direct sunlight

absorption properties of nanohorn-based nanofluids. In fact, carbon nanohorns show an absorption peak located in the ultraviolet region, whose tail, that extends all over the base fluid transparency range, can be recognized in the short-wavelength side of Fig. 5

Optical losses simulation

To give a realistic assessment of the potential of the direct absorption nanofluid solar collector, optical losses occurring when sunlight hits a thin transparent tube have been calculated. We considered different tube materials: a low-cost borosilicate glass (BK7), a quartz glass (fused silica), which is characterized by a higher UV transmittance, and, finally, a transparent thermoplastics (Poly-Methyl MethAcrylate-PMMA, which is better known with the commercial name of Plexiglas). The transmittance spectrum of the considered tube materials shown in Figure 6 allows one to appreciate the differences among their spectral characteristics.
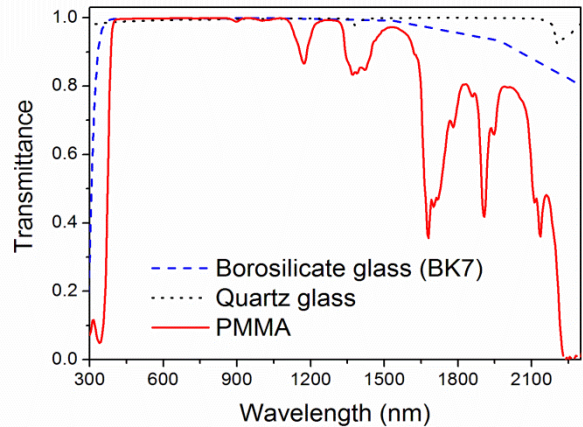
Figure 6: Transmittance spectrum of the investigated tube materials, for the reference thickness of 10 mm.

Optical losses simulations have been performed using the Zemax™ ray-tracing software in non-sequential mode, tracing 10 million rays. For the input light, we considered a source with sunlight spectrum [15] and sunlight 0.27° half-angle divergence [16]. The geometrical model we used for the tube is a simple cylinder with 47 mm inner diameter and 1.6 mm wall thickness. Sunlight hits the pipe perpendicularly to its longitudinal axis. The obtained irradiance on the tube inner surface has been used as input light for the nanofluid calculations described in the next sections.

Figure 7 shows the ray-tracing simulations for the empty PMMA half-tube, while Figure 8

shows the irradiance distribution on the half-tube inner surface. The light absorption by the tube is taken into account for thermal calculations, as detailed in the following sections.
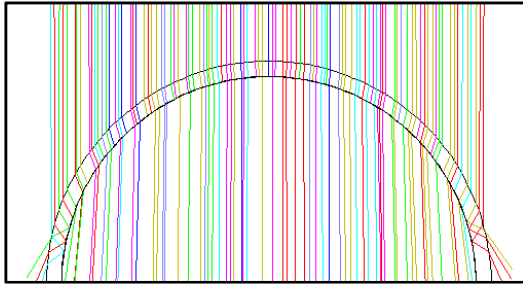

Figure 7: Ray tracing simulations for the PMMA tube. Different colors refer to different wavelengths of the input light. For clarity reasons, only few wavelengths are shown in the figure (380, 495, 550, 650, 750, 850 and 1050 nm).
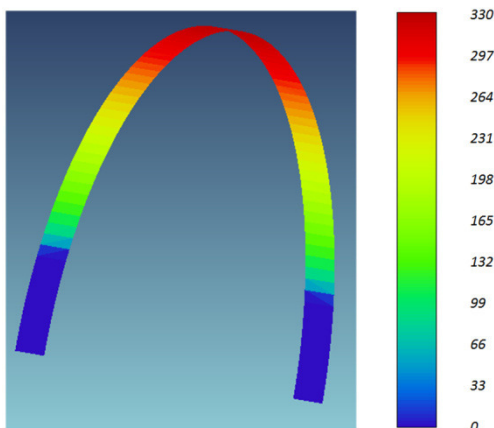

Figure 8: Irradiance distribution for on the inner half-tube surface. The tube is made in PMMA. Maximum irradiance (deep red) is 330 W/cm^2 and decreases as the polar angle increases.

RESULTS AND DISCUSSION

Nanofluid concentration

Figure 9 shows the variation of the collector efficiency as a function of nanoparticle concentration. Absorption coefficient of nanofluid can be adjusted by varying the concentration of nanoparticles. In this section, the concentration of nanoparticles in water-based nanofluids has been varied from 0.004 g/l to 0.05 g/l, with the constant inlet velocity of 0.001 m/s.

As can be observed from the Figure 9, increasing nanoparticle concentration initially increases the collector efficiency up to a

maximum value. Then, a further increase in the concentration leads to decrease in the collector efficiency.

This phenomenon can be explained as follows. Generally speaking, increasing nanoparticles concentration increases nanofluid absorption coefficient and consequently increases the collector optical absorption. Using a certain concentration causes complete absorption of the incoming solar radiation, but beyond this maximum value, any further increase of the nanofluid absorption coefficient results in a shorter length for the radiation attenuation inside the fluid. This higher concentration of absorbed energy causes an increase of the surface temperature and, therefore, the heat losses to the environment increase as well. The increase of the surface temperature due to the increased nanoparticle concentration can be observed in Figure 10.
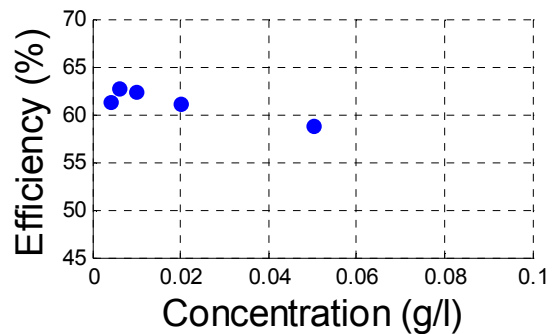

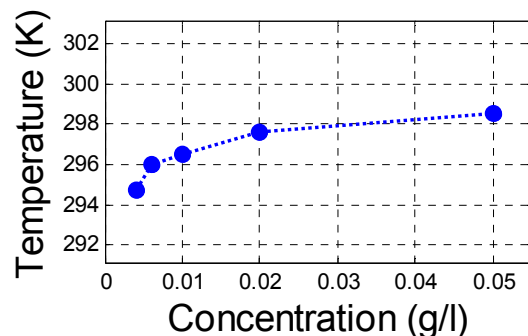*Figure 9: effect of nanoparticle concentration on the efficiency of collector.*

Figure 10: average top temperature of the single tube collector as a function of nanoparticle concentration

Tube Material

Application of three different materials: BK7, fused silica and PMMA, as transparent material for construction of tube is investigated, using their transmittance and thermophysical properties.

The effect of the transparent material can be seen from different points of view:

1- Overall transmittance for the solar radiation.
2- Spectral transmittance, that determines the spectral intensity of the passed light and so, affects the mean absorption coefficient of the nanofluid weighted by the incoming radiation.
3- Heat transfer characteristics of the material: the smaller the thermal conductivity of the material, the smaller the heat losses to the environment.

Data of Sample A4 are used to evaluate the effect of the tube material. The modelling is performed considering the actual properties of these materials, and including the heat loss to the ambient due to natural and forced convection.

Overall transmittance of the considered materials differs each other about 1%. Thus, the dominating effect of the different materials would be their heat conduction capabilities.

Figure 11 and 12 compare the efficiencies of solar collector with different tube materials.

The efficiency of a solar thermal collector is normally expressed as a function of the ratio x by the following expression:

$$\eta = a_0 - a_1 x - a_2 x^2 I \qquad (16)$$

$$x = \frac{T_{mean} - T_a}{I} \qquad (17)$$

In equation (16) the a_0 coefficient represents the optical efficiency, while a_1 and a_2 (positive values) govern the linear and non linear components of thermal losses.

Figures 11 and Figure 12 clearly indicate that the collector with PMMA has better performance as compared to two considered glasses. This results arises from its lower thermal conductivity which, in turn, decreases the heat conduction from the fluid side to the ambient side. By comparing Figure 11 and Figure 12 it is observed that with increasing heat loss coefficient, the superiority of the advantage of using PMMA over the two glass materials is more evident. However, plastic suffers from a lower stability at high temperature and a lower strength, which could limit its use in evacuated tube configuration. So considering its lower cost, PMMA and generally a high transmittance plastic can be a suitable candidate to be used as transparent material instead of glass where high temperatures are not needed and when there is a high heat loss coefficient.
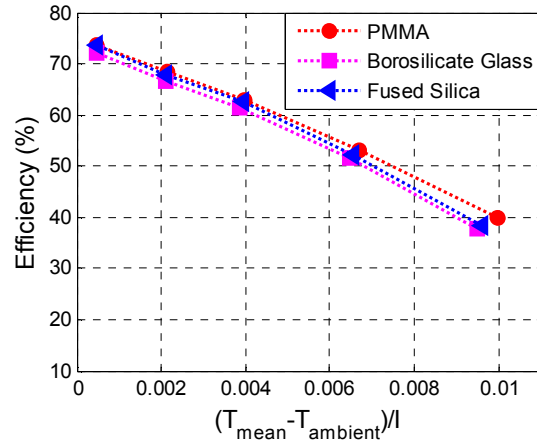

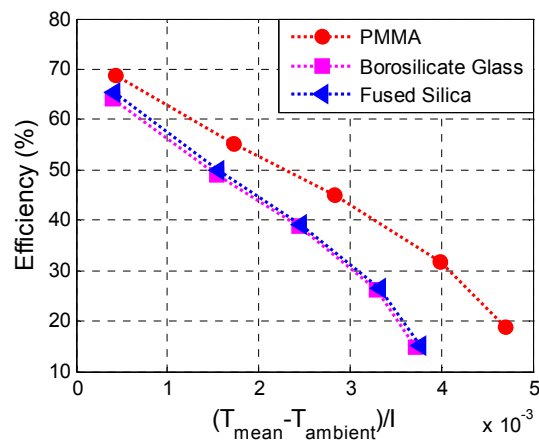Figure 11: Collector Efficiency for the different tube materials with natural convection

Figure 12: Collector Efficiency for the different tube material with forced convection

Comparison between water-based and glycol-based nanofluids:

Attenuation of sunlight in pure water is higher than in pure glycol, which results in slightly higher absorption coefficient of water-based nanofluids with respect to glycol-based nanofluids.

However in solar thermal collectors, water is often replaced by glycol or water/glycol mixtures, both to protect against freezing and to achieve higher outlet temperatures, because of the lower specific heat capacity of glycol itself. Furthermore, its higher boiling point makes possible to use it in higher temperature systems and in solar collectors with higher sunlight concentration ratio.

Figure 13 compares the efficiency of glycol-based and water-based samples. It can be seen that the efficiency of the water-based nanofluid is higher, which happens because of the lower heat losses due to the lower surface temperature. However, it can be seen in Figure 14 that higher outlet temperatures can be achieved using glycol for any flow rate.
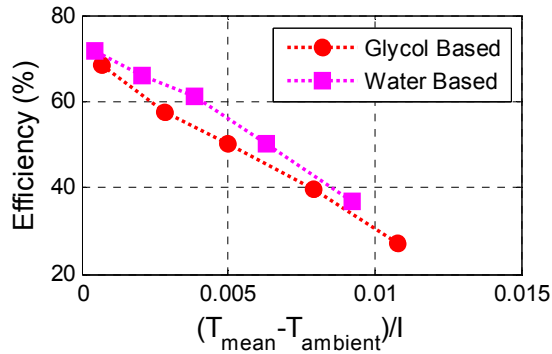
Figure 13: comparison of the collector efficiency for glycol-based and water-based nanofluid with nanoparticle concentration= 0.02 g/l
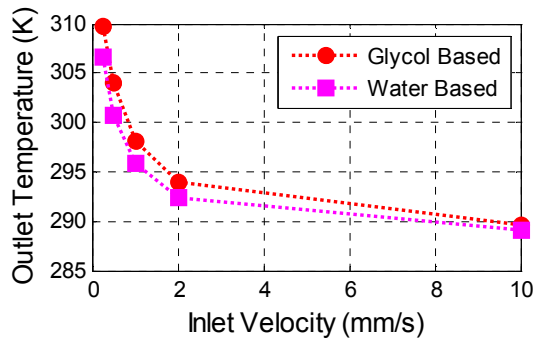

Figure 14: comparison of outlet temperature for glycol-based and water-based nanofluid

Figures 15 and 16 show the outlet temperature profile for the single tube collector with natural convection and forced convection heat loss, respectively. As it can be observed, if thr heat loss increases, the maximum temperature gets close to the center of the fluid. This characteristic favourably compares the direct absorption configuration with respect to selective surface absorbers in which the maximum temperature is always reached at the surface. The evolution of the temperature along the pipe can be seen in Figure 18.
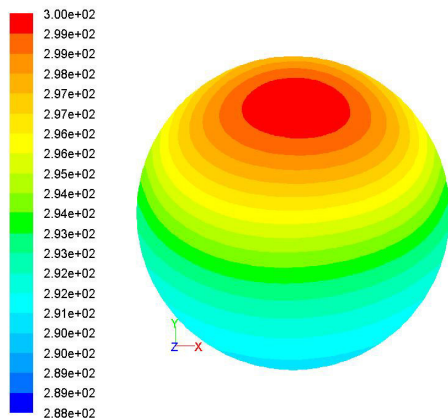

Figure 15: outlet temperature profile for the single tube solar collector, with the A4 nanofluid sample and forced convection heat loss
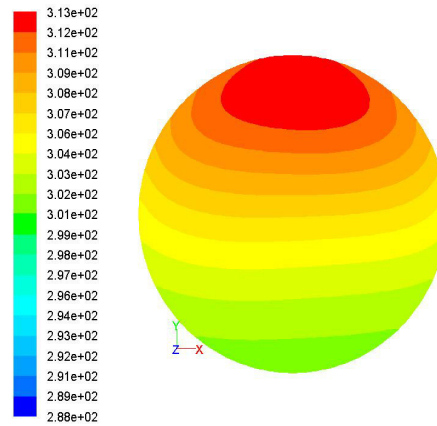

Figure 16 outlet temperature profile for the single tube solar collector, with the A4 nanofluid sample and natural convection heat loss
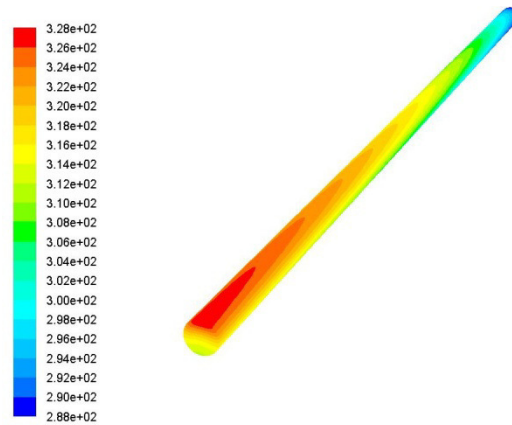

Figure 18: evolution of temperature along the pipe

COMMENTS

The efficiency diagrams of Figures 11 and 12 show a performance of single tube collectors that is significantly different from a standard non-glazed collector. While a typical flat, indirect adsorption, unglazed solar thermal collector would have a_1 value (transmittance value) in the order of 10-15 $W/m^2/K$ [17], the same value derived for our system is 42 $W/m^2/K$. This means that the single tube direct absorption collector (STDA) has significantly higher thermal losses in relation to the same aperture area (net area over which the irradiance is collected). This is mainly due to the higher external surface of the cylindrical tube configuration in comparison to a common flat plate one (FP). The ratio of the external surface of the STDA to the flat plate is naturally π, hence the actual global transmittance of the solar collector, defined on the difference between mean water temperature and outdoor air temperature, and on the external surface of the tube, is on the order of 13 $W/m^2/K$. Following this point of view, the most

important limit of this configuration is the augmented heat transferring surface rather than the heat transfer coefficient. The bottom part of the tube is not useful for absorption and should be insulated.

A possible plus of the cylindrical configuration is not considered in this paper, and could emerge into a dynamic simulation. Considering the two angles that describe the relative position of the Sun to the collector, azimuth and tilt angle, the symmetry of the cylinder could offer a constant aperture area in relation to one of the two. For example, if the cylinder is fixed in the north-south direction, the normal component of the aperture area is constant in relation to the azimuth angle (Figure 19).
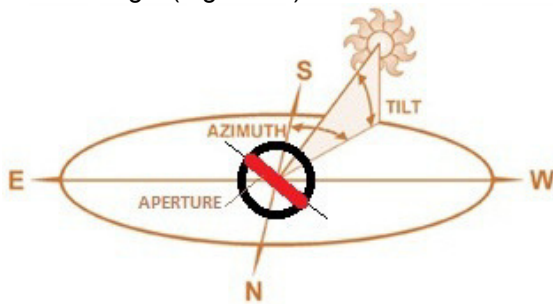

Figure 19 The cylindrical configuration presents an aperture surface of constant area relative to one of the two angles that describe the sun position

The simulations performed and shown here demonstrate the basic idea of having the highest temperature inside the fluid and thus achieving a possible advantage, but underline the limits of the cylindrical configuration. Future possible improvements of this setup include a lower global transmittance (obtainable, for example, by a thicker plastic tube), the use of a tube with different section, for example elliptical, the application of back insulation and the application of a back reflecting surface, as in the case of concentration system.

Economical considerations and LCA (life cycle assessment) will add important elements to the evaluation of this family of collectors.

CONCLUSIONS

Nanofluid-based direct absorption solar collectors and the application of various transparent materials of the collector tube were investigated by ray-tracing simulation using Zemax™ software and a 3D heat transfer analysis, by FLUENT™ software. The single tube collector with presence of natural and forced convection heat loss has been modelled to study the effect of heat loss coefficient. It has been observed that using PMMA (representative of a high transmittance plastic) as tube material,

the efficiency of the collector would be higher with respect to glass, due to the lower thermal conductivity of PMMA.

Increasing concentration of nanoparticles initially increases the efficiency of the collector but, beyond a certain value of concentration, a further increase in nanoparticle concentration will decrease the efficiency due to the higher surface temperature.

Finally, the effect of the base fluid has been studied by comparing water-based and glycol-based nanofluids. It has been observed that water-based nanofluids produce higher values of efficiency. On the other hand, the use of glycol as base fluid allows to reach higher outlet temperatures. So, when high temperature is not required, a water-based nanofluid (or a mixture of water-glycol with higher percentage of water) is more suitable.

ACKNOWLEDGMENTS

Nomenclature

A_o	Inner tube's outer area (m^2)
$D_{c,i}$	inner diameter of cover (outer tube) (m)
$D_{c,o}$	outer diameter of cover (outer tube) (m)
D_i	inner diameter of inner tube (m)
D_o	outer diameter of inner tube (m)
h_a	Convective heat transfer coefficient from the outer tube to the ambient (W/m^2K)
I	Irradiance (W/m^2)
L	Length of solar receiver (m)
Nu	Nusselt Number (-)
Pr	Prantdl Number (-)
q_h	volumetric energy flux (W/m^3)
Q_loss	heat loss to the ambient (W)
r	Length of the light path (m)
R	Inner radius of inner tube (m)
Ra	Rayleigh Number (-)
T_a	Ambient Temperature (K)
T_{mean}	Average temperature of water in the collector [K]
T_{sky}	Sky Temperature (K)
T_{roof}	Roof Temperature (K)
V	Volume (m^3)
x, y	Coordinates (m)

Greek Symbols

α_m	mean absorption coefficient (1/m)
α_λ	spectral absorption coefficient (1/m)
τ_λ	spectral transmittance of the tube's wall (-)
τ_x	overall transmittance of the tube's wall as a function of dimensionless coordinate, x/R (-)
σ	Stephen Boltzmann constant (W/m^2K^4)
ε_c	Emissivity of the cover (-)
εi	Emissivity of the inner tube (-)
η	Efficiency of solar collector
$\emptyset$	energy flux (W)
$\vec{v}$	velocity vector (m/s)
ρ	density (kg/m^3)
μ	dynamic viscosity (Pa s)

REFERENCES

[1] DIRECTIVE 2009/28/EC OF THE EUROPEAN PARLIAMENT AND OF THE COUNCIL of 23 April 2009 on the promotion of the use of energy from renewable sources and amending and subsequently repealing Directives 2001/77/EC and 2003/30/EC

[2] ESTIF, European Solar Thermal Industry Federation, http://www.estif.org/policies/res_directive/

[3] DTI Microgeneration Strategy 2006, http://webarchive.nationalarchives.gov.uk/+/htttp://www.dti.gov.uk/files/file27575.pdf

[4] Repubblica Italiana, Decreto Legislativo 8 febbraio 2007, n.20, Attuazione della direttiva 2004/8/CE sulla promozione della cogenerazione basata su una domanda di calore utile nel mercato interno dell'energia, nonche' modifica alla direttiva 92/42/CEE, Gazzetta Ufficiale della Repubblica Italiana n. 54, 6 febbraio 2007

[5] Scarpa, R. , Willis, K., Willingness-to-pay for renewable energy: Primary and discretionary choice of British households' for micro-generation technologies, Energy Economics 32 (2010) 129–136.

[6] Ardente, F., Beccali, G., Cellura, M., Lo Brano, V.,"Life cycle assessment of a solar thermal collector: sensitivity analysis, energy and environmental balances" Renewable Energy 30 (2005) 109–130.

[7] Omid Mahian, Ali Kianifar, Soteris A. Kalogirou, Ioan Pop, Somchai Wongwises, A review of the applications of nanofluids in solar energy, International Journal of Heat and Mass Transfer 57 (2013) 582–594.

[8] Theunissen, P.H., Beckman, W.A., Solar Transmittance Characteristics of Evacuated Tubular Collectors with Diffuse Back Reflectors, Solar Energy, 35 (1985), 4, pp. 311320.

[9] Kalogirou, S.A. Solar thermal collectors and applications , Progress in Energy and Combustion Science, 30 (2004), 231-295.

[10] Duffie, J.A., Beckman, W.A.,Solar Engineering of Thermal Processes John Wiley and Sons New York, (2006).

[11] Çengel, Y.A. Heat Transfer - A Practical Approach, pp. 486-488. second ed. McGraw-Hill New York, (2004).

[12] ASHRAE handbook: HVAC applications. Atlanta (GA): ASHRAE, 1999.

[13] M.C.J. Large, D.R. McKenzie, M.I. Large, Incoherent reflection processes: a discrete approach, Optics Commun. 128 (1996) 307–314.

[14] E. Sani, L. Mercatelli, S. Barison, C. Pagura, F. Agresti, L. Colla, P. Sansoni, Potential of carbon nanohorn-based suspensions for solar thermal collectors, Solar Energy Materials and Solar Cells, 95 (2011) 2994-3000.

[15] CIE Technical Report No. 85, Solar Spectral Irradiance, 1989.

[16] D. Buie, A. G. Monger, and C. J. Dey, Sunshape distributions for terrestrial solar simulations, Solar Energy, 74 (2003) 113–122.

[17] SPF Test reports, SPF Institut für Solartechnik • Oberseestrasse 10 • CH-8640 Rapperswil, CH, www.solarenergy.ch